The electronic structure of Al_3Ni

1995 J. Phys.: Condens. Matter 7 4865

(http://iopscience.iop.org/0953-8984/7/25/011)

J. Phys.: Condens. Matter 7 (1995) 4865–4874. Printed in the UK

The electronic structure of Al_3Ni

G Cubiotti†, E E Krasovskii‡, O V Slobodyan‡, Yu N Kucherenko‡ and V N Antonov‡

† Sezione di Fisica Teorica, Dipartimento di Fisica, Universita di Messina, PO Box 50, I-98166 S Agata di Messina, Italy

‡ Institute of Metal Physics, National Academy of Sciences of Ukraine, Vernadsky Street 36, 252142 Kiev, Ukraine

Received 21 September 1994, in final form 7 March 1995

Abstract. *Ab initio* calculations of the electronic structure of the Al_3Ni compound have been performed, by use of the actual orthorhombic structure and of two different model structures having cubic symmetry. The self-consistent extended linear augmented plane-wave method is used. The details of the calculations are presented and the results are discussed and compared with experimental data. The calculated density of electron states (DOS) turns out to represent well the experimental ultraviolet photoelectron spectrum. We conclude that model structures should be used with some caution, because they can yield DOS curves that differ substantially from the real energy distribution of the valence electrons.

1. Introduction

Owing to their high strength, hardness, high melting point, oxidation resistance, and unusual electronic and magnetic properties, intermetallic compounds consisting of a transition metal and aluminium are the subject of important industrial developments. This has initiated a great deal of experimental as well as theoretical investigation on the electronic structure of these compounds, their cohesive properties, phase transitions, etc [1–11]. In [2] the band structure of Me–Al compounds (Me = V, Cr, Mn, Fe, Co, Ni) has been calculated using the linear Korringa–Kohn–Rostoker (LKKR) method. In [6] the linear muffin-tin orbitals (LMTO) method has been used to study the TiNi compound. All these compounds have a relatively simple crystal structure (a cubic lattice with two or four atoms per unit cell). The $MeAl_3$ crystals (Me = Sc, Ti, Zr), which have a more complicated lattice ($D0_{22}$ structure, eight atoms per unit cell), have been studied in [3, 4].

The Al_3Ni compound has an orthorhombic lattice with 16 atoms per unit cell. So far there have been no attempts to calculate the electronic structure of Al_3Ni based on its actual crystal lattice. The Al–Ni alloys are of current interest. Several band-structure calculations have been performed on this system [7–11], which, however, were restricted to the ordered intermetallic compounds Ni_3Al and NiAl with the cubic lattices of Cu_3Au and CsCl type, respectively. In the case of Al_3Ni a simplified model crystal structure has been employed to study trends in the electronic structure and in cohesive properties of ordered Al–Ni compounds as a function of stoichiometry [7]. There the augmented spherical-wave (ASW) method has been used.

In [12] the results of both experimental (ultraviolet photoelectron spectroscopy (UPS)) and theoretical (LMTO) studies of the electronic structure of Mg–Me and Al–Me compounds (Me = Ni, Cu, Zn) have been reported. In [7, 12] the Al_3Ni compound was treated as

0953-8984/95/254865+10$19.50

a cubic crystal with Cu_3Au-type lattice. The theoretically obtained well defined double-peak shape of the density-of-states (DOS) curve was in disagreement with the measured UPS spectrum. In order to explain this discrepancy, an additional study is needed.

In the present work we report the results of the band-structure calculations for the Al_3Ni compound with its real orthorhombic lattice. The other aim of this work is to study how sensitive is the energy distribution of the valence electrons to changes in crystal structure, i.e. what is the effect of the real crystal lattice being substituted by a model one, still retaining the composition of the solid.

This paper is organized as follows. In section 2 we give the comparative description of the Al_3Ni crystal structure and of the two model structures explored. In section 3 the method of calculation and the computational details are described. The calculated results for all the structures considered are presented and discussed in section 4. Conclusions are presented in section 5.

2. Al_3Ni crystalline structure and model structures

The Al_3Ni compound has the orthorhombic $D0_{20}$ structure (space group *Pnma*) with 16 atoms per unit cell [13] (figure 1): four Ni atoms and 12 Al atoms. Because of the different atomic surroundings there are two non-equivalent positions for Al atoms, which are denoted as Al-1 (four atoms) and Al-2 (eight atoms). The lattice parameters are $a = 0.661\,15$ nm, $b = 0.733\,64$ nm and $c = 0.481\,18$ nm. The positions of the atoms in the unit cell are presented in table 1. Each Ni atom is surrounded by nine Al atoms: three atoms of Al-1 type at distances of 0.245–0.272 nm and six atoms of Al-2 type at distances of 0.244–0.259 nm, whereas the Ni–Ni distance is relatively large and equal to 0.380 nm. Each of both Al-1 and Al-2 atoms has only three Ni atoms as the nearest neighbours.

Table 1. Positions of atoms (given in units of the lattice constants a, b and c) in the unit cell of Al_3Ni.

Sort of atom	x	y	z
Ni	0.0	0.0	0.0
	0.262	0.5	0.890
	0.5	0.0	0.390
	0.762	0.5	0.5
Al-1	0.120	0.5	0.360
	0.142	0.0	0.530
	0.620	0.5	0.030
	0.642	0.0	0.860
Al-2	0.305	0.197	0.089
	0.305	0.803	0.089
	0.457	0.303	0.589
	0.457	0.697	0.589
	0.805	0.197	0.301
	0.805	0.803	0.301
	0.957	0.303	0.801
	0.957	0.697	0.801

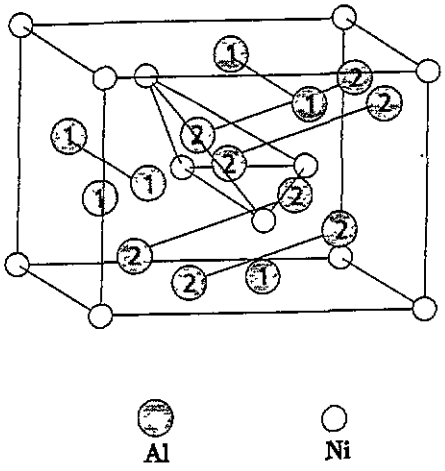

Figure 1. The unit cell of the Al_3Ni compound. Non-equivalent Al atoms are denoted by symbols 1 and 2.

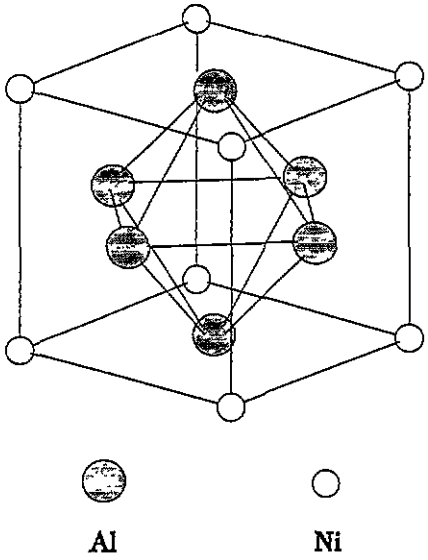

Figure 2. The unit cell for the Cu_3Au-type lattice (model (I)).

In order to study the effect of using the model crystal lattice instead of the real one, we have chosen two different model structures, both having cubic symmetry and four atoms per unit cell. In what follows we have denoted them as model (I) and model (II).

Model (I) has a lattice of Cu_3Au type ($L1_2$ structure, space group $Pm3m$) (figure 2). This model has already been used for energy band calculations in [7, 12]. Because in [7] and [9] calculational methods have been used that differ from the method used in the present work, we consider the model (I) as a test to check the effect of the method used.

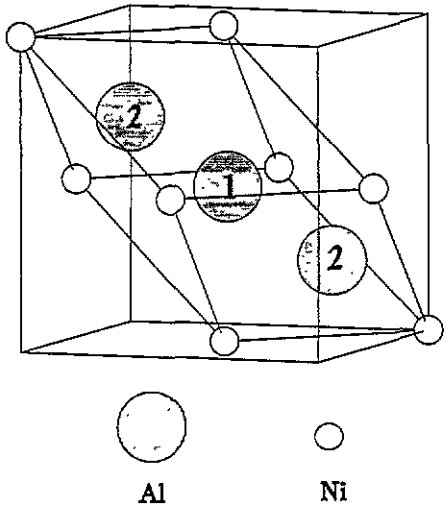

Figure 3. The unit cell for the BiF_3-type lattice (model (II)).

As model (II) we have chosen the BiF_3-type lattice ($D0_3$ structure, space group $Fm3m$) (figure 3). This lattice is not so close packed as that of model (I) and here Al atoms occupy two non-equivalent positions in the unit cell as is the case for the real Al_3Ni structure.

The lattice parameters for both model structures have been chosen so that the average volumes per atom are equal to that in the real crystal structure: $a = 0.38840$ nm for model (I) and $a = 0.61656$ nm (for the cubic cell) for model (II). The nearest interatomic distances for both model structures are given in table 2. One can see that the Ni–Ni distance in (I) is very close to that in the real structure; the Ni–Al distance, however, exceeds that in Al_3Ni. In contrast, in (II) the Ni–Ni distance is considerably larger than that in the real structure; and the Ni–Al distance falls within a realistic distance range. It should be noted that both models differ significantly from the orthorhombic structure in the coordination numbers and in the symmetry of the local atomic environment.

Table 2. Interatomic distances (nm) for the model structures.

Interatomic distance	Model (I)	Model (II)
d(Ni–Ni)	0.3884	0.4360
d(Ni–Al)	0.2746	0.2669

3. Description of the method

Among the methods presently used to calculate band structures, methods that treat accurately singular one-electron crystal potentials are either time consuming (augmented plane wave (APW), Korringa–Kohn–Rostoker (KKR)) or have rather narrow energy interval of validity, about 1 Ryd (LMTO, linear augmented plane wave (LAPW)). Apart from this it has been shown [14] that the LAPW method is not capable of producing accurate wavefunctions even when the eigenenergies are correct. The origin of this shortcoming is that the shape of the LAPW wavefunction inside the muffin-tin (MT) sphere is uniquely determined by its plane-wave expansion in the interstitial. Because of this, when one extends the basis set to achieve convergence, the plane waves being added, which are necessary to represent the wavefunction in the interstitial, can spoil the representation of the wavefunction inside the sphere. This means that the correct plane-wave expansion in the interstitial cannot, generally, be achieved within the LAPW. Slater's APW method is devoid of this shortcoming; the wavefunction is flexible, i.e. the radial parts of the angular momentum decomposition inside the sphere can be changed without changing the plane-wave expansion. This is achieved at the expense of the wavefunction being discontinuous in slope at the sphere boundary. In this work we use the extended LAPW method (ELAPW) [15], which employs wavefunctions that are flexible and at the same time continuous in slope.

The ELAPW differs from the usual LAPW method proposed by Andersen [16] in that a set of additional basis functions $\{Z_{lmn}\}$, which vanish in the interstitial region, is added to the LAPW basis set. The scheme is analogous to that described by Singh [17]. In the usual LAPW, the basis set $\{\psi_i\}$ is uniquely determined by the set of energy parameters $\{E_{vl}\}$. Inside the sphere at the origin the energy-independent APW is written as

$$\psi_i(r) = \sum_{lm} A_{lmi} u_{li}(r) Y_{lm}(\hat{r}) \tag{1}$$

$$A_{lmi} = 4\pi i^l Y^*_{lm}(\hat{K}_i) \tag{2}$$

$$K_i = k + G_i \tag{3}$$

where k is the Bloch vector and G_i is the reciprocal lattice vector. The radial functions, u_{li}, are linear combinations of the solution of the radial Schrödinger equation for the energy E_{vl}, ϕ_{vl} and its energy derivative at this energy, $\dot{\phi}_{vl}$:

$$u_{li}(r) = c_{li}\Phi_{vl}(\tilde{D}_{li}, r) \tag{4}$$

$$\Phi_{vl}(D, r) = \phi_{vl}(r) + \omega_l(D)\dot{\phi}_{vl}(r). \tag{5}$$

Here $\tilde{D}_{li}$ is the radial logarithmic derivative of the Bessel function

$$\tilde{D}_{li} \equiv S\frac{j_l'(K_i r)}{j_l(K_i r)}\bigg|_{r=S} \tag{6}$$

S is the sphere radius and D is the logarithmic derivative of the function $\Phi_{vl}(D, r)$. The radial functions $u_{li}(r)$ satisfy the matching conditions at the sphere boundary

$$u_{li}(S) = j_l(K_i S) \qquad u_{li}'(S) = j_l'(K_i S). \tag{7}$$

In the ELAPW we introduce an additional set of energy parameters, $\{E_{\mu l}\}$, and employ the radial functions $\phi_{\mu l}$ and $\dot{\phi}_{\mu l}$ to construct $2(2l+1)$ new basis functions for each l:

$$Z_{lmn}(r) = z_{ln}(r)Y_{lm}(\hat{r}) \qquad n = 1, 2. \tag{8}$$

The radial functions z_{ln} have both zero value and zero slope at the sphere

$$z_{ln}(S) = 0 \qquad z_{ln}'(S) = 0 \tag{9}$$

which is achieved by the following linear combinations:

$$z_{l1}(r) = \phi_{\mu l}(r) - \frac{\phi_{\mu l}(S)}{\Phi_{vl}(D_\mu, S)}\Phi_{vl}(D_\mu, r) \tag{10}$$

$$z_{l2}(r) = \dot{\phi}_{\mu l}(r) - \frac{\dot{\phi}_{\mu l}(S)}{\Phi_{vl}(D_{\dot{\mu}}, S)}\Phi_{vl}(D_{\dot{\mu}}, r). \tag{11}$$

Here D_μ and $D_{\dot{\mu}}$ are logarithmic derivatives of the $\phi_{\mu l}$ and $\dot{\phi}_{\mu l}$ respectively.

Now we use the set of localized functions, $\{Z_{l_0 m1}, Z_{l_0 m2}\}$, to construct the set of additional APW, $\{\xi_{l_0 j};\ j = 1, 2, \ldots, 2(2l+1)\}$. We define the column vector

$$Z_n \equiv (Z_{l_0,-l_0,n}, Z_{l_0,1-l_0,n}, \ldots, Z_{l_0,l_0,n})^{\mathrm{T}} \qquad \mathbf{Z} \equiv (Z_1^{\mathrm{T}}, Z_2^{\mathrm{T}})^{\mathrm{T}}$$

and the vector Ψ whose components are the APW constructed with the energy parameters $\{E_{vl}\}$, $\Psi = (\psi_1, \psi_2, \ldots, \psi_{2(2l+1)})$:

$$\xi = \hat{\mathbf{B}}\mathbf{Z} + \Psi \qquad \hat{\mathbf{B}} = [\hat{\mathbf{L}}|\hat{\mathbf{R}}]. \tag{12}$$

The matrices $\hat{\mathbf{L}}$ and $\hat{\mathbf{R}}$ have $2l+1$ columns and $2(2l+1)$ rows each:

$$L_{jm} = a_j A_{l_0 mj} \qquad R_{jm} = b_j A_{l_0 mj}. \tag{13}$$

If we choose $a_j = j_{l_0}(K_j S)/\Phi_{\mu l_0}(\tilde{D}_j)$ and $b_j = a_j \omega_{\mu l_0}(\tilde{D}_j)$, we find the $\{\xi_{l_0 j}\}$ to be a set of usual (constructed according to equations (1)–(6)) APW based on the same energy parameters as the LAPW set, $\{\psi_i\}$, except for the angular momentum l_0 ($E_{\nu l_0}$ is replaced by the $E_{\mu l_0}$). In other words, if one unites two LAPW basis sets (each containing N APW) that differ in a single energy parameter, say $E_{\nu l_0}$, the resulting set contains (no more than) $N + 2(2l + 1)$ linearly independent functions. For computational purposes we use the ξ functions instead of the Z ones, as this allows us to avoid the complexity of the matrices (in the case where the crystal lattice has inversion symmetry), and to change the computer code of the LAPW method only slightly. It should be noted that having a finite set of ψ it is not always possible to select $2(2l + 1)$ functions so as to construct the matrix $\hat{\mathbf{B}}$ with a non-zero determinant. In this case the additional basis set contains less than $2(2l + 1)$ ξ functions.

In the case of noble metals the ELAPW method yields accurate eigenvalues over the energy range from the bottom of the valence band up to 4 Ryd above the Fermi level [15] (the eigenvalues differ from those calculated with Slater's APW by less than 2 mRyd). Now we examine the accuracy and the convergence properties of ELAPW and LAPW as applied to the orthorhombic Al_3Ni crystal. The number of the usual APW, N_{APW}, is determined by a dimensionless parameter, KS, where K is the largest reciprocal lattice vector, i.e. $|G_i| \leqslant K$, and S is the radius of the smallest MT sphere ($S = 2.2$ au). The additional basis set comprises all the spherical waves with $l \leqslant 3$ for the three types of atom, so that the dimension of the Hamiltonian matrix is $N_{APW} + 3 \times 2 \times (l_{max} + 1)^2$. The energy parameters, $E_{\nu l}$ and $E_{\mu l}$, are listed in table 3.

Table 3. The energy parameters of the ELAPW calculation, $E_{\nu l}$ and $E_{\mu l}$ (in rydbergs, relative to muffin-tin zero), and the logarithmic derivatives, $D_{\nu l}$. For all l the additional parameters, $E_{\mu l}$, were taken at the D branch next to the νth. All $E_{\mu l}$ were chosen so that $D_{\mu l} = -12.0$.

	l	$E_{\nu l}$	νth branch	$D_{\nu l}$	$E_{\mu l}$	μth branch
Al-1	0	1.23	3s	−5.7	8.6	4s
	1	1.23	3p	−2.0	9.0	4p
	2	1.23	3d	0.0	8.7	4d
	3	1.23	4f	1.8	13.6	5f
Al-2	0	1.24	3s	−5.4	9.1	4s
	1	1.24	3p	−2.0	9.5	4p
	2	1.24	3d	0.1	9.1	4d
	3	1.24	4f	1.8	14.2	5f
Ni	0	0.38	4s	−1.0	12.6	5s
	1	0.38	4p	0.3	13.7	5p
	2	0.39	3d	−3.0	5.8	4d
	3	0.37	4f	2.3	14.6	5f

To compare the two methods we calculate the energy expectation value in the interstitial of the wavefunction of the lowest valence state at the k-point Γ. The value is defined by

$$E(\text{out}) = \int_{\text{out}} \Psi^* \hat{H} \Psi \, d\mathbf{r} \Big/ \int_{\text{out}} \Psi^* \Psi \, d\mathbf{r}$$

where the integration is over the interstitial region. If the wavefunction is exact, then E(out) coincides with the eigenvalue. Thus we consider the difference between the well

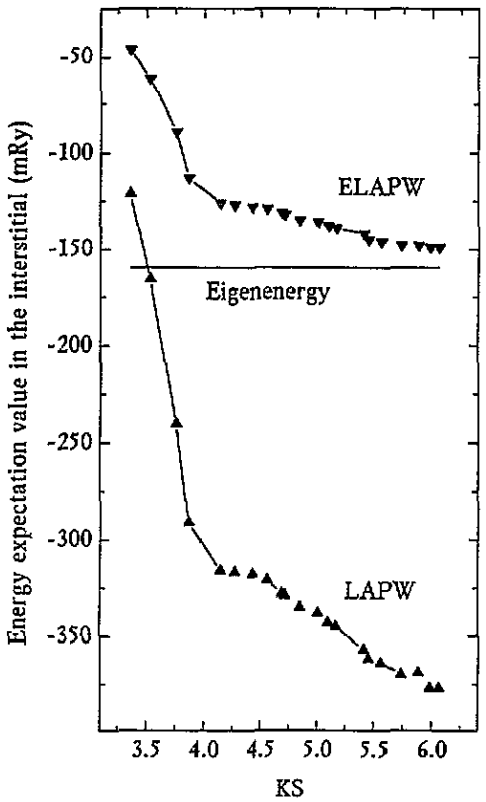

Figure 4. The convergence of the energy expectation value, E(out), for the lowest valence state in the point Γ.

converged value of E(out) and the eigenvalue, ΔE, to be a criterion of the accuracy of the wavefunction.

The dependence of E(out) on KS for both methods is shown in figure 4. The value of KS changes from $KS = 3.4$ ($N_{APW} = 97$) to $KS = 6.1$ ($N_{APW} = 545$). The shape of the curves is typical (see [14]). The deviations of the converged E(out) values from the eigenvalue are $\Delta E_{ELAPW} = 10$ mRyd, $\Delta E_{LAPW} = 225$ mRyd. The ELAPW wavefunction turns out to be 20 times 'more precise' than the LAPW one. Figure 4 suggests that the rate of convergence of the wavefunctions in the two methods is practically the same. Yet the ELAPW eigenvalue converges faster than the LAPW one: for the state in question the former converges to within 1 mRyd at $KS = 3.5$, while the latter does so at $KS = 5.5$. The converged ELAPW eigenvalue coincides with that calculated by Slater's APW method, whereas the LAPW eigenvalue is 8 mRyd higher.

The Al_3Ni band structure has been calculated self-consistently using the exchange–correlation potential proposed by Hedin and Lundqvist [18]. The tetrahedron method [19] has been used to obtain DOS curves. The number of k-points in the irreducible part of the Brillouin zone (BZ) was 75 for the orthorhombic crystal (192 tetrahedra), 35 for model (I) (64 tetrahedra) and 174 for model (II) (512 tetrahedra). For the orthorhombic crystal KS was equal to 5.4 ($N_{APW} = 397$), for model (I) $KS = 6.5$ ($N_{APW} = 179$) and for model (II) $KS = 8.0$ ($N_{APW} = 229$). The energy parameters used for the model structures were close to those listed in table 3.

4. Discussion of the calculated results

The calculated local partial DOS for the orthorhombic Al_3Ni compound are presented in figure 5. The energy distribution of the valence electron states forms one high peak at energy −2.7 eV (Ni d states) on the smooth background (Al s and p states). In general, the non-equivalent Al atoms have a very similar local DOS; one can find only some differences in the fine structure of the DOS curves. Note that the chemical binding is predominantly provided by the interaction of the Ni d states with the Al p states, whereas the Al s states are localized at lower energies at the bottom of the valence band. The distribution of the p states in the energy range between −1 and −4 eV shows that the Al-1 states interact with Ni d states over all the width of the d band, especially in the middle of the d band. The interaction of the Al-2 states with Ni d states occurs at the bottom and at the top of the d band. As can be seen from table 4, the non-equivalent Al atoms have different Madelung charges; moreover, the Al-1 atom has a value of positive Madelung charge that is larger than that of the Al-2 atom (in spite of the larger value of the Al-1 MT sphere radius). These results allow us to conclude that the chemical states of the non-equivalent Al atoms are significantly different.

Table 4. Comparison of the parameters and gross features of the band structure for three versions of the crystal lattice. E_d is the centre of gravity of the occupied d states. E_b is the bottom of the valence band. The charge that enters into the Madelung potential is defined as $Q = Z - Z_{el} + V\rho_0$, Z = charge of the nucleus, Z_{el} = electronic charge in the MT sphere of volume V and ρ_0 = electronic density in the interstitial.

Lattice structure		*Orthorhombic*	*Model (I)*	*Model (II)*
MT sphere radii S (nm):	Al-1	0.1284	0.1373	0.1333
	Al-2	0.1254	0.1373	0.1333
	Ni	0.1164	0.1164	0.1164
Madelung charge Q:	*Al-1*	*3.25*	*3.05*	*3.07*
	Al-2	3.10	3.05	3.13
	Ni	2.60	2.52	2.54
Electronic density in the interstitial ρ_0 (electron/nm^3)		209.4	202.6	202.7
$E_F - E_d$ (Ryd)		0.197	0.171	0.166
$E_F - E_b$ (Ryd)		0.805	0.822	0.818
$N(E_F)$ *(states/(Ryd×structure unit))*		17.32	23.41	31.42

The comparison of calculated results obtained for different crystal lattices shows that the differences in the chemical states of the non-equivalent Al atoms in the model (II) lattice are weak. The values of the constant electronic density in the region outside the MT spheres are very close for all three structures considered. This is provided by the choice of the same average atomic density for all structures. One can see from table 4 that the orthorhombic Al_3Ni structure has the deepest location of the Ni d states and the lowest value of the DOS at the Fermi level. This suggests that the actual structure must have lower total energy than both model structures.

In figure 6 the calculated DOS are presented in comparison with the experimental UPS spectrum [12]. It can be seen that only the orthorhombic structure yields a single wide peak (displaying the Ni d states) in the spectrum. Both model structures have double-peak DOS, reflecting the energy positions of the d states of different symmetry. For example, for model (I) the peak at −2.9 eV is formed by the degenerate Ni t_{2g} states bonded with

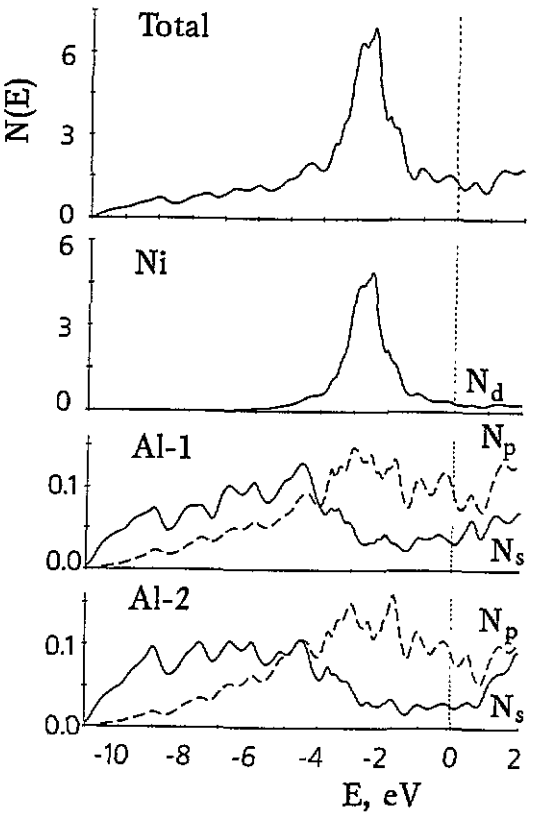

Figure 5. The total and the local partial DOS for orthorhombic Al_3Ni. The units are states/(eV×structure unit) for the total DOS and states/(eV×atom) for the local DOS.

Al p states, while the sharp peak at −2.0 eV displays the non-bonding Ni e_g states. In the orthorhombic lattice, owing to the low symmetry of the local atomic environment of Ni atoms, the degeneracy of the d states is cancelled and these states are distributed in a rather wide energy interval.

5. Conclusions

We have performed *ab initio* calculations of the electronic structure of the Al_3Ni compound by using the actual orthorhombic structure and two different model structures having cubic symmetry.

Our results on model (I) confirm the earlier ASW [7] and LMTO [12] results, which are in disagreement with experiment.

We have shown that in application to the actual structure of Al_3Ni the ELAPW method is much more precise than the LAPW. The accuracy of the wavefunctions is especially important in studying the optical properties, which is in progress.

The DOS curve derived from the actual structure is in agreement with the UPS measurements [12]. We conclude that the symmetry of the local environment of Ni atoms is the leading factor in formation of the Ni d DOS shape. The low symmetry of the actual crystal lattice eliminates the energy separation of the e_g and t_{2g} Ni d states, which results in a

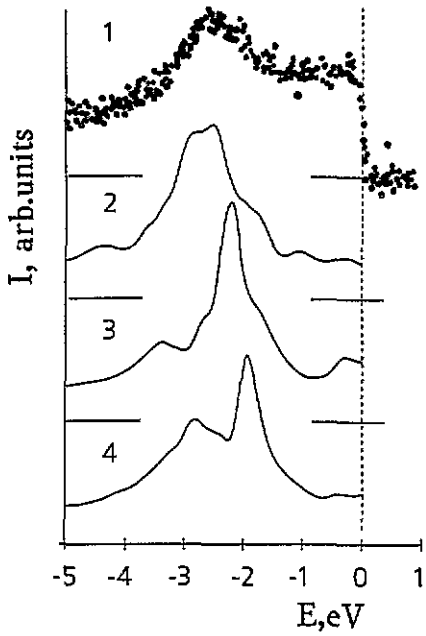

Figure 6. *The comparison of the experimental* Al_3Ni UPS *spectrum* (1) *with the calculated* results for the orthorhombic lattice (2), model (II) (3), and model (I) (4).

single broad peak in the DOS curve instead of its double-peak shape in the model structures. The separation is present in both model structures, in which the interatomic distances are different but the cubic symmetry is retained.

References

[1] Lahdeniemi M, Ojala E and Okochi M 1981 *Phys. Status Solidi* b **108** K61
[2] Muller Ch, Blau W and Ziesche P 1983 *Phys. Status Solidi* b **116** 561
[3] Hong T, Watson-Yang T J, Freeman A J, Oguchi T and Xu Jian-hua 1990 *Phys. Rev.* B **41** 12462
[4] Xu J-H and Freeman A J 1990 *Phys. Rev.* B **41** 12553
[5] Chang Y A, Pike L M, Liu C T, Bilbrey A R and Stone D S 1993 *Intermetallics* **1** 107
[6] Erschbaumer H, Podloucky R, Rogl P, Temnitschka G and Wagner R 1993 *Intermetallics* **1** 99
[7] Hackenbracht D and Kubler J 1980 *J. Phys. F: Met. Phys.* **10** 427
[8] Buiting J J M, Kubler J and Mueller F M 1983 *J. Phys. F: Met. Phys.* **13** L179
[9] Yegorushkin V Ye, Kulmentyev A I and Rubin P E 1985 *Fiz. Met. Metalloved.* **60** 421
[10] van der Heide P A M, Buiting J J M, ten Dam L M, Schreurs L W M, de Groot R A and de Vroomen A R 1985 *J. Phys. F: Met. Phys.* **15** 1195
[11] Min B I, Freeman A J and Jansen H J F 1988 *Phys. Rev.* B **37** 6757
[12] Andrews P T, Millar S C, Cubiotti G, Kucherenko Yu, Yaresko A N and Antonov V N 1993 *J. Phys.: Condens. Matter* **5** 1935
[13] Pearson W B 1967 *A Handbook of Lattice Spacing and Structures of Metals and Alloys* (Oxford: Pergamon)
[14] Krasovskii E E, Nemoshkalenko V V and Antonov V N 1993 *Z. Phys.* B **91** 463
[15] Krasovskii E E, Yaresko A N and Antonov V N 1994 *J. Electron Spectrosc.* **68** 157
[16] Andersen O K 1975 *Phys. Rev.* B **12** 3060
[17] Singh D 1991 *Phys. Rev.* B **43** 6388
[18] Hedin L and Lundqvist B I 1971 *J. Phys. C: Solid State Phys.* **4** 2064
[19] Lehmann G and Taut M 1972 *Phys. Status Solidi* b **54** 469